Hindawi
Advances in Civil Engineering
Volume 2024, Article ID 5588833, 18 pages
https://doi.org/10.1155/2024/5588833

Research Article

A Comparative Study of Seismic Performance Evaluation of Reinforced Concrete Frame Structures Using Chinese and African Seismic Codes

Musaab Suliman and Liang Lu

Department of Disaster Mitigation for Structures, Tongji University, 1239 Siping Road, Shanghai 200092, China

Correspondence should be addressed to Musaab Suliman; musaab@tongji.edu.cn

Received 4 December 2023; Revised 16 January 2024; Accepted 9 February 2024; Published 22 February 2024

Academic Editor: Chunfeng Wan

The evaluation of various earthquake codes, it is one of the significant challenges in the study area of earthquake engineering. However, according to the literature review, most research works have not addressed comparing Chinese and African seismic codes. Therefore, the purpose of this study is to identify each code's advantages by comparing assessment of the seismic efficacy of moment resistance frame reinforced concrete (MRF-RC) frames using four different codes: the Ethiopian Building Code Standard (EBCS-8), the Egyptian Code for Design and Construction of Reinforced Concrete Structures (ECP-201), the Algerian Seismic Regulations (RPA-99), and the Chinese Code for Seismic Design of Buildings (GB-50011), the first three are the major codes used in Africa. The seismic provisions of these codes are compared and evaluated using nonlinear time-history analysis (NL-THA) and nonlinear static pushover to validate the results. These analyses are performed on four MRF-RC frame models with different heights. The results include various parameters that reflect the seismic performance of the structures. The study revealed that the Chinese code is more conservative and overestimates seismic performance compared with African codes. However, the Chinese code can be applied in African projects considering the African soil classifications, and seismic weight are adjusted to meet the African design criteria.

1. Introduction

With the promotion of the "One Belt and Road Initiatives" proposal, Chinese engineering firms are more involved in international projects. This means that domestic designers have to understand international design standards. A key area of focus is the earthquake resistance requirements, which are essential for structure configuration. Therefore, this area is getting more attention [1]. Due to its high seismic activity, China has updated its seismic code GB-50011-2010 [2] several times since 1959 to ensure safety and resilience [3].

Africa has moderate seismic activity compared to other parts of the world [4]. However, some areas are more prone to earthquakes than others, while others are almost free. The northern part of Africa, especially Egypt and Algeria, has experienced several strong earthquakes. The most powerful was a 7.3 local magnitude quake that hit El Asnam in Algeria's Tell Atlas in 1980. Before the 1990s [5], some minor earthquakes were reported in northern Egypt with local magnitude of 5 or less [6, 7]. Recently, a 4.4 body wave magnitude quake was also felt in the Hawassa region of Ethiopia. This earthquake happened in 2016 [8], and many adjacent cities and towns felt the tremors [9].

Egypt published its first seismic code (ECP-1989) in 1989 [10]. It was revised in 1993 (ECP-1993) and 2003 (ECP-2003) to address the shortcomings of the previous versions [11]. The ECP-2003 seismic code considers the building's response spectra and soil modulus seismic regions [10, 12]. Algeria established its first seismic regulation (RPA-81) in 1980. It was revised several times, most recently to RPA-99/Version 2003 [13] after the 2003 Zemori earthquake [14]. Ethiopia modified its code (ESCP1–83) in 1983 and revised it to EBCS 8 : 1995 [15] based on recent earthquake records. A council to revise the code was established in 2013 [16].

The earthquake response of reinforced concrete (RC) structures planned by modern regulations has been studied by various researchers, focusing on American and European structures. A numerical analysis of a 4-story RC structure according to the International Building Code 2003 was conducted by Kueht and Hueste [17]. The European standard was used by Panagiotakos and Fardis [18] to evaluate the behavior of RC buildings. Ile and Reynouard [19] proposed a constitutive model with fixed orthogonal cracks and the smear crack method to evaluate the periodic behavior of RC structures. Studies [20, 21] examined the earthquake behavior of typical RC frames designed according to the Chinese standard (GB-50011-2010) [2]. Young et al. [22] compared the seismic behavior of RC structures designed based on GB-50011 and European standards.

This research aimed to compare the seismic codes for concrete frame structures in China and Africa, considering the increasing influence of Chinese construction companies in Africa. These companies have funded and built many tall buildings in Africa, such as the Iconic Tower in Egypt, which is 385 m high [23, 24]. These projects may use the Chinese building standards, which have been developed based on their previous construction experience [25]. Therefore, this study aims to identify code differences by comparing the assessment of the seismic efficacy of moment resistance frame reinforced concrete (MRF-RC) using Chinese and African codes. The study aims to fill the research gap in the literature on comparing and evaluating Chinese and African seismic codes by measuring the seismic performance of MRF-RC frames.

2. Methodology

The designs of RC buildings with 2-, 4-, 8-, and 12-story with moment resisting systems are compared under different seismic intensity levels. The comparison includes member sizes, vibrational properties, earthquake design loads, and material usage. Next, nonlinear finite element analysis models are created to assess the earthquake behavior of the designs. Seismic design codes were compared based on permitted analysis methods, zoning scheme, site class, the dynamic baseline period of the building, response reduction factor, importance factor, minimum lateral design force, allowable interstory drifts, and design response spectrum. A nonlinear behavior time-history analysis was performed on each building, and several key indicators were conducted to evaluate the performance of the four buildings.

2.1. Structure Model. The structure type chosen here is the RC moment-resistant frame structure, a common building structure. Based on the HAZUS Directory [26], building ties are categorized by height or the number of stories. Therefore, buildings with 2, 4, 8, and 12 stories have been selected to model low-rise, mid-rise, and high-rise buildings. The structures have a regular shape in layout and elevation, with four spans along the X-axis and four spans along the Y-axis, as shown in Figure 1(a) direction, and a story height of 3.5 m, as demonstrated in Figure 1(b). These structures are being designed as office buildings. The dead load of the floors is 3 kN/m^2, not including the self-weight of the building's members. The live load of the roof floor is 0.75 kN/m^2, and the live load of the other floors is 2.5 kN/m^2. This study adopts HRB400 steel with E and ∂ values of 210 GPa and 0.02 and concrete with 30 MPa compressive capacity.

The frames are designed using the standard Chinese GB-50011 and African norms following the Eurocode to design concrete structures [25]. The structural analysis and design were conducted with the assistance of ETABS software [27]. ETABS is widely used in engineering design offices and was endorsed by Abdo [28] to analyze RC multistory buildings. Shell elements are used for the panels, and frame components are used for the beams and columns. The supports are located at the foundation level. The total beam and column stiffness are considered in the analysis of all models. The complete quadratic combination (CQC) was applied to integrate the behavior of different modes according to the recommendations of EBCS-8, ECP-201, RPA-99, and GB-50011-2010. Tables 1 and 2 show the section and reinforcement design of the form frame. For each axis (X or Y), the center of mass was allocated an accidental eccentricity of 5% (relative to the corresponding level dimension).

2.2. Nonlinear Dynamic Analysis (NL-DA). A powerful tool for this purpose is incremental dynamic analysis (IDA), which involves performing the nonlinear time-history analysis (NL-THA) for a range of ground acceleration intensities and recording the structural response. NL-THA provides more realistic results about how a specific structure performs under seismic excitation [29], accounting for the structural element's nonlinear behavior and the ground acceleration dynamic characteristics. However, NL-THA requires a suitable intensity measure (IM) to characterize the ground motion [30]. Nazri and Alexander [31] highlighted that peak ground acceleration (PGA) is a frequently utilized parameter, the IDA curve can be generated through the correlation between the interstory drift ratio and PGA.

Nine pairs of seismic ground motions acceleration with various seismicity levels are chosen for each building is showed in Table 3. These ground motion pairs are employed for NL-THA. A total of 36 pairs of raw seismic data are obtained from the PEER NGA website, whose response spectrum agrees with the response spectra for the four-character scheme. SeismoMatch uses spectral matching to transform accelerometer data into an analogous response spectrum. The program depends on the wavelet method several authors proposed [32–34]. The wavelet algorithm method for aligning response spectra is employed in earthquake engineering to customize recorded ground movements to match desired seismic parameters. This process entails breaking down the motion into components specific to certain frequencies using wavelet transformation. These components are then optimized using algorithms such as enhanced colliding bodies optimization (ECBO) to reduce the difference between the actual and target spectra. The components are subsequently modified and recompiled into a fresh ground motion time history. This approach guarantees that the altered ground motion adheres to design specifications while maintaining

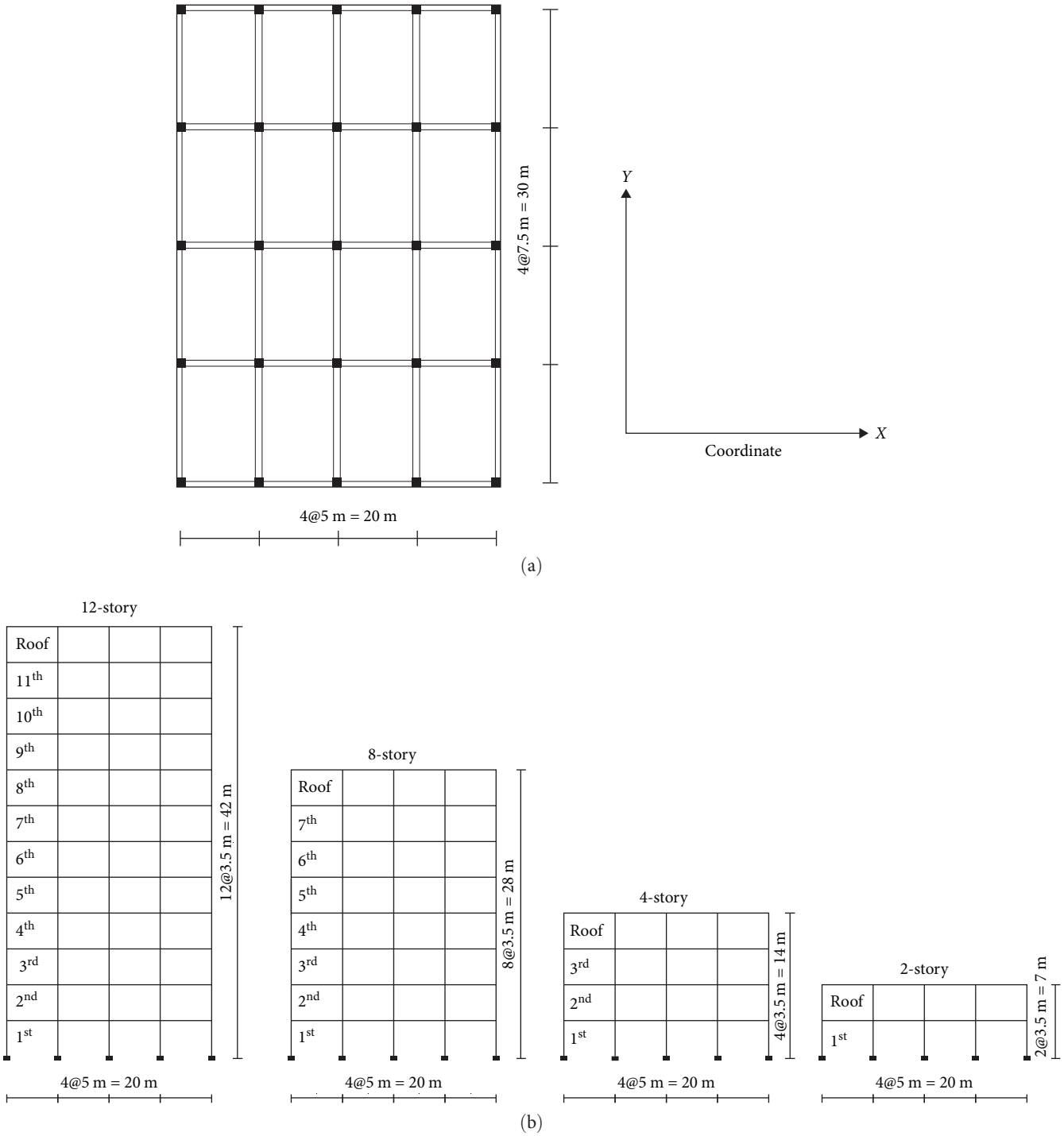

Figure 1: (a) Typical floor plan of model buildings and (b) 2-, 4-, 8-, and 12-story model frames.

the original motion's traits [35]. The period range for spectral alignment using wavelet algorithms generally encompasses the range of periods that are pertinent to the design and analysis of structures under seismic loading. For this study, the intermediate period range is set between 0.2 and 2 s, during which the spectral shape exhibits a linear decrease. These ground motions were scaled to 0.2 g for time history analysis. Figure 2 illustrates the matched response spectrum of chosen records with the design response spectra of the four codes.

The Takeda model [36], as shown in Figure 3, is employed in the incremental nonlinear dynamic analysis to simulate the flexural response's hysteretic behavior. This approach effectively mimics the cyclic behavior observed in plastic hinges and is key to reproducing the decreasing strength and stiffness commonly seen in concrete structural components [38].

where K_i: initial stiffness, Δ_y: yield displacement, and Δ_m: maximum displacement.

Table 1: Beam section and reinforcement design of frames.

Building	Story	GB-50011-2010			African code		
		Cross-section (mm)	Rebar top (T) bottom (B)	Stirrup	Cross-section (mm)	Rebar top (T) bottom (B)	Stirrup
2-Story	1–2	550 × 300	6Ø16(*T*) 6Ø16(*B*)	Ø8@200 mm	550 × 300	5Ø20(*T*) 5Ø16(*B*)	Ø8@150 mm
4-Story	1–4	600 × 300	5Ø20(*T*) 4Ø20(*T*)	Ø8@200 mm	600 × 300	6Ø20(*T*) 4Ø20(*B*)	Ø8@150 mm
8-Story	1–8	600 × 350	6Ø20(*T*) 5Ø20(*B*)	Ø8@100 mm	600 × 350	8Ø20(*T*) 6Ø20(*B*)	Ø10@150 mm
12-Story	1–12	600 × 400	6Ø25(*T*) 6Ø25(*B*)	Ø8@100 mm	600 × 400	7Ø25(*T*) 5Ø25(*B*)	Ø10@150 mm

Table 2: Column section and reinforcement design of frames.

Building	Story	GB-50011-2010			African code		
		Cross-section	Rebar	Stirrup	Cross-section	Rebar	Stirrup
2-Story	1–2	500 × 300	10Ø16	Ø8@100 mm	500 × 300	10Ø20	Ø8@100 mm
4-Story	1–4	550 × 550	22Ø20	Ø8@100 mm	550 × 500	28Ø20	Ø8@100 mm
8-Story	1–4	650 × 650	20Ø25	Ø8@100 mm	650 × 650	24Ø25	Ø8@100 mm
	5–8	600 × 600	10Ø25	Ø8@100 mm	600 × 600	14Ø25	Ø8@100 mm
12-Story	1–4	750 × 750	30Ø25	Ø8@100 mm	750 × 750	36Ø25	Ø8@100 mm
	5–8	700 × 700	18Ø25	Ø8@100 mm	700 × 700	22Ø25	Ø8@100 mm
	9–12	650 × 650	14Ø25	Ø8@100 mm	650 × 650	16Ø25	Ø8@100 mm

Table 3: The earthquake ground motion characteristics data used for analysis.

Level	PGA (g)	Earthquake	Station	Year	M_w	EPD/km	T_g/s
Low	0.21	North Palm Springs	Morongo Valley	1986	6.0	10.1	1.90
	0.31	Whittier Narrows	E-Grand Avenue	1987	6.0	9.1	0.70
	0.29	Morgan Hill	Gilroy Array #6	1994	6.2	11.8	1.20
Moderate	0.48	Loma Prieta	Coyote Lake Dam	1989	6.9	21.8	0.65
	0.51	Loma Prieta	Saratoga-Aloha Avenue	1989	6.9	11.7	1.80
	0.59	North Palm Springs	5,070	1986	6.0	8.2	1.10
High	0.60	Coalinga	Pleasant Valley P.p	1983	5.8	17.4	0.65
	0.84	Northridge	Rinaldi	1994	6.7	7.1	1.05
	1.04	Cape Mendocino	Cape Mendono	1992	7.1	8.5	2.00

2.3. Nonlinear Static Analysis (NL-SA). The study employs nonlinear static analysis to assess a structure's capability of withstanding a powerful earthquake. The nonlinear static analysis refers to the pushover analysis. This well-established technique generates a capacity curve representing the structure's capacity in force and deformation before failure. This approach aims to plot a curve illustrating the force and deformation a building can tolerate before collapse. This technique helps engineers design or retrofit existing buildings to resist seismic damage. The pushover analysis reveals crucial information about the structure's strength, stiffness, and ductility, which can then be used to determine potential deficiencies and propose remedies. Improving these response parameters tends to enhance the earthquake resilience of the structure.

The pushover analysis method was used, specifically employing the SPO2IDA tool to estimate the strength ratio (R) and ductility (μ) curve of the frames [39], which presents an effective approach to estimate the seismic demand and capacity of systems dominated by the first mode of vibration across a range from semielasticity behavior to total failure, as shown in Figure 4. It correlates the curve of static pushover (SPO) empirically with its associated for IDA. This method uses empirical formulas to link the R strength ratio of the one

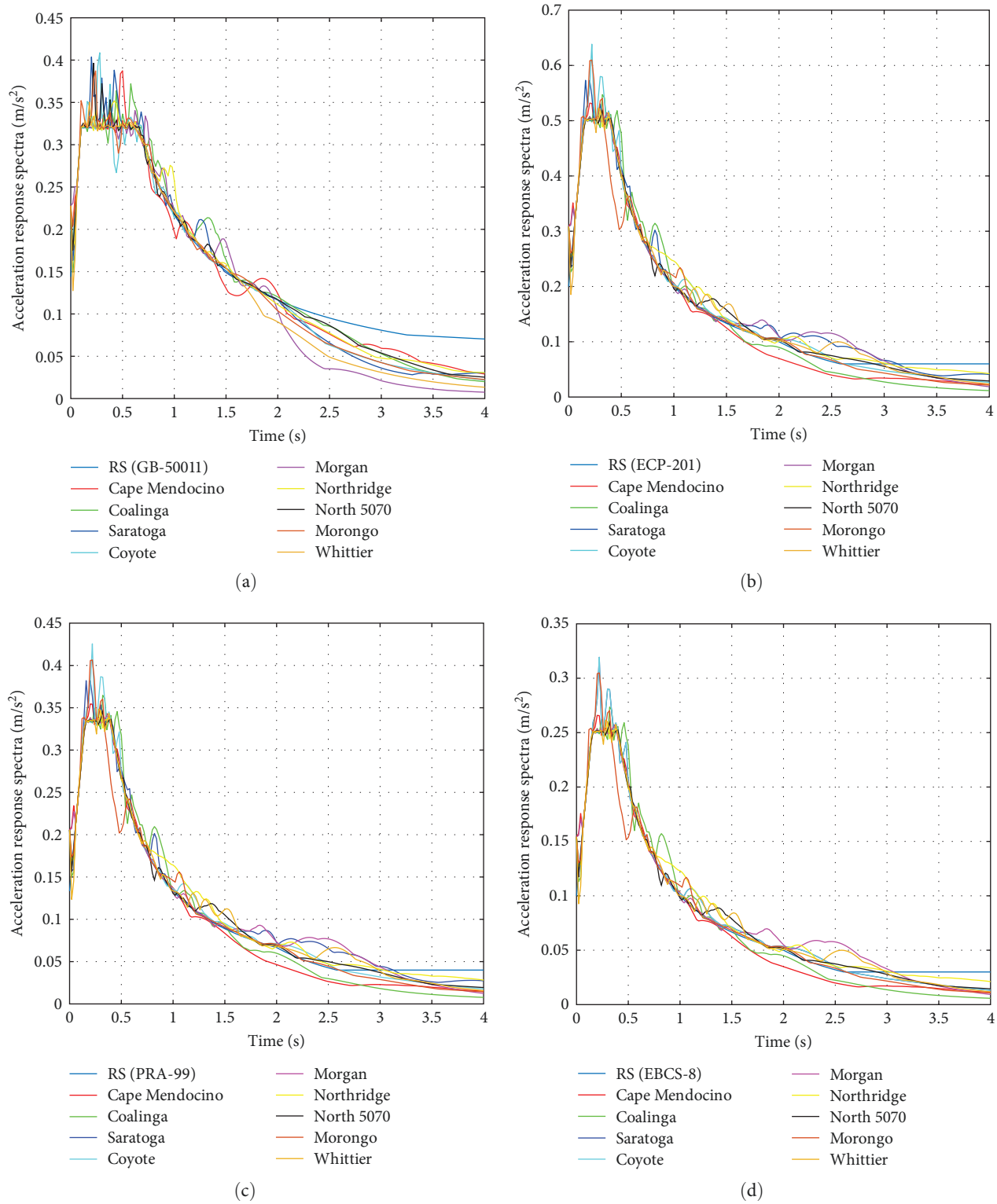

Figure 2: The matched response spectrum of selected ground records with design response spectra: (a) GB-50011; (b) ECP-201; (c) RPA-99; and (d) EBCS-8.

degree of freedom (1DOF) system to the elastic spectrum for a specific ground acceleration, T its seismic period, and μ its ductile ratio. Those formulas between the R, T, and μ were already derived for different types of SPO basis curves and incorporated into the tools. The outcome is to transform the pushover curve variables for the multiple degrees of freedom (MDOF) into a comparable 1DOF system and then calculate the (IDA) curves.

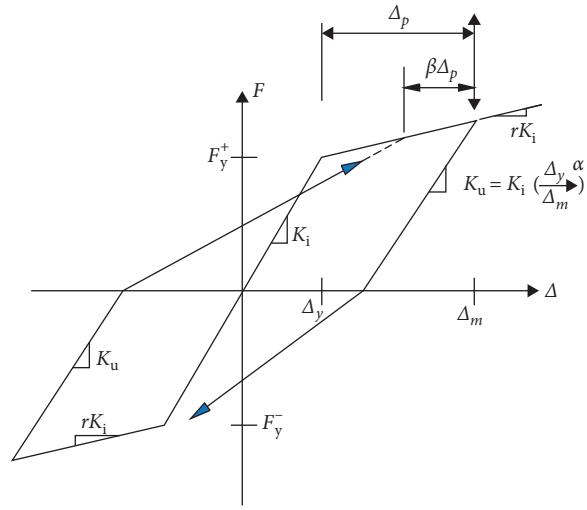

Figure 3: Takeda hysteretic model [37].

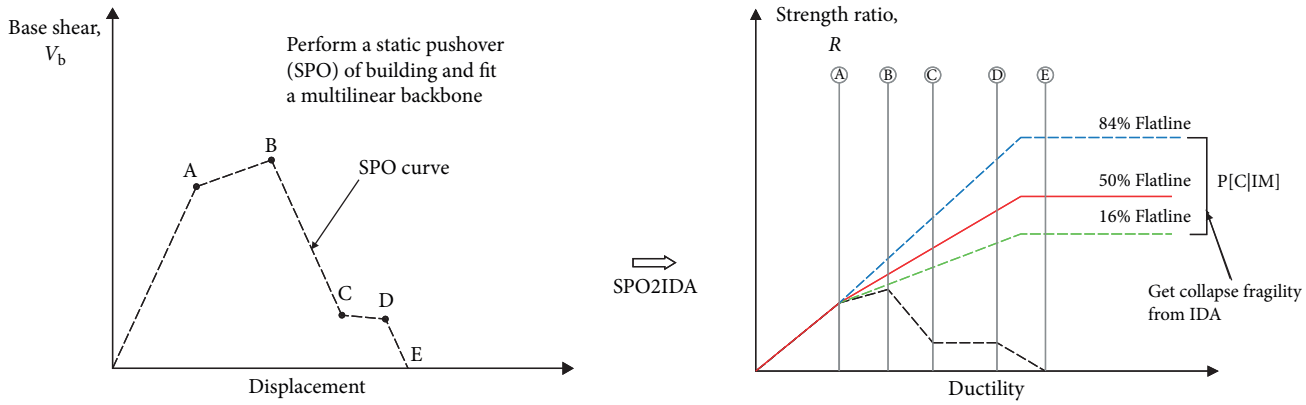

Figure 4: The SPO2IDA software developed by Cornell and Vamvatsikos [39], was used to estimate the IDA curves, which links the SPO curve and the IDA.

$$R = \frac{F_{el}}{F_y} = \frac{Sa(T_1)}{Sa_y}, \tag{1}$$

$$\mu = \frac{\Delta^*}{\Delta_y^*}. \tag{2}$$

F_{el} is the elastic spectrum demand on an 1DOF system with period T_1 under ground acceleration excitation, and F_y represents the yield force of that system, Δ^* denotes the maximum displacement response and Δ_y^* signifies the yield displacement. Put simply, R signifies the ratio of strength for the first mode spectrum acceleration of a particular ground acceleration or design spectra, $Sa(T_1)$, and the spectrum acceleration yield of the equivalent 1DOF, Sa_y. As illustrated in Figure 4, the relationship pushover analysis curve and its corresponding IDA percentiles (i.e. 16th, 50th, or median and 84th) were quantified empirically. The SPO–IDA approach allows the translation of the basic parameters of an MDOF system into an equivalent SDOF oscillator, thus facilitating the estimation of seismic demand (i.e. IDA traces) based on well-established empirical R-T-μ relationships.

In the pushover analysis conducted using ETABS, the characteristics of concentrated plastic hinges are key. As illustrated in Figure 4, Point A represents the initial yielding of structural elements, which is determined by their moment–curvature relationship. At Point C, hinge deformation signifies a reduction in strength, potentially leading to sudden structural collapse [40]. In this analysis, beams are assumed to carry no axial load. However, for columns, the axial load is calculated as the permanent load plus 0.25 or 0.5 of the live load, in line with African and Chinese standards, respectively. The length of the plastic hinge is crucial in determining the maximum rotation, derived from the peak curvature. The plastic rotation for each hinge is determined by Equation (3) [41]:

$$\theta_p = \left(\Phi_u - \Phi_y\right) \cdot L_p. \tag{3}$$

Here, Φ_u and Φ_y denote the yield and ultimate moment curvatures, and L_p is the length of the plastic hinge.

According to ATC-40 [42], the length of the plastic hinge should be half the depth of the section in the load direction, a guideline known to produce conservative results. This approach is adopted in this study to calculate the hinge length. Thus,

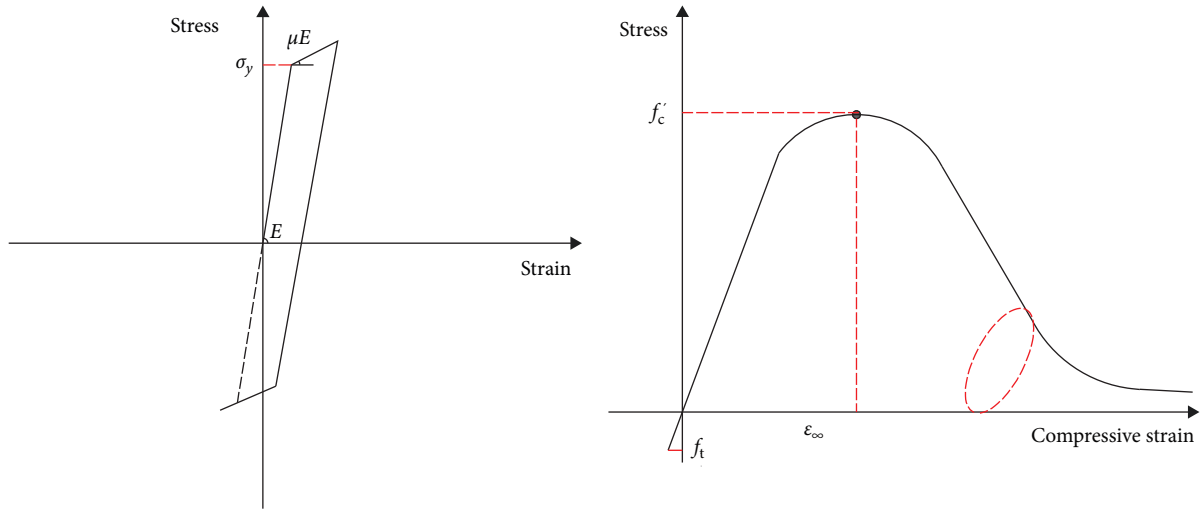

(a) (b)

FIGURE 5: Constitutive material models: (a) steel and (b) concrete [43].

$$L_p = 0.5\,h, \tag{4}$$

h: section depth of the element, beam, or column.

As a result, with gravity loads uniformly distributed across the beam, potential plastic hinges are considered at both ends of columns and beams. In ETABS, similar to FEMA 356's plastic hinges, column axial-moment hinges (P-M3) and beam bending moment hinges (M3) are defined at the extremities of these elements.

For inelastic material as shown Figure 5(a) illustrates the constitutive material models for steel and concrete. The bilinear rubbery model with kinematic strain reinforcement was employed to stiffen steel. The model requires three parameters: modulus of elasticity (E), yield strength (σ_y), and strain-hardening coefficient (∂). This study adopts HRB400 steel with E and ∂ values of 210 GPa and 0.02, respectively. The longitudinal and annular yield strengths are 570 and 400 MPa, respectively. Figure 5(b) shows that the uniaxial static confined model was used to represent the concrete material. The model needs four parameters: compressive capacity (f_c'), tensile capacity (f_t), maximum strain (ε_{co}) corresponding to (f_c'). The f_c', f_t, and ε_{co} values are 30, 2.4 MPa, and 0.002, respectively.

2.4. Fragility Curve. Seismic impact hazards on structural models can be estimated analytically using fragility curves, which are beneficial methods for estimating the likelihood of failure to any structural system. Fragility curves can also help in making retrofit decisions. The fragility of buildings is evaluated using time-history IDA, and drifts will be used to track severe damage that could cause structural collapse. The deflection percentage can then be computed as shown in Equation (5).

$$\%\text{Drift} = \frac{\text{Roof displacement}}{\text{Building height}} \times 100. \tag{5}$$

Fragility curves are developed based on several seismic parameters, among which the PGA parameter is used in both IDA and fragility curve development. The damage condition for the four models is determined by the performance levels: operational phase OP, immediate occupancy IO, damage control DC, life safety LS, and collapse prevention CP, which correspond to drift values of 0.5%, 1%, 1.5%, 2%, and 2.5%, respectively, based in FEMA-P-695 process [44]. Two main factors are required to create fragility curves: the average (α) and standard deviation (σ). The following equation in Equation (6), which Ibrahim and El-Shami [45] have used.

$$P\left[\frac{D}{PGA}\right] = \varnothing\left(\frac{\ln(PGA) - \alpha}{\sigma}\right), \tag{6}$$

where $\varnothing$ is the standard normal cumulative distribution function, σ is the standard deviation of the logarithm, α is the average value, and D is the damage state.

3. Comparison of Seismic Provisions

All buildings were assumed to have rigid subsoil. The properties of rigid soil include a shear wave velocity between 180 and 360 m/s, a standard penetration strength between 15 and 50, and an unconsolidated shear resistance between 70 and 100 KPa. Comparing the two investigated codes reveals that rigid soil corresponds to Soil C in ECP-201 and EBCS-8, to Soil D in the GB-50011 code, and S3 in the RPA-99 code. The soil factor S in ECP-201, EBCS-8, and RPA-99 is identical and varies according to soil type and building proximity to the Mediterranean Seashore. For the buildings under investigation, S is 1.5. On the other hand, the soil factor ζ_a in GB-50011, it is dependent on soil type and has a value of 1.3. The intended use of office buildings. All four codes

classify them as standard occupancy. Each code assigns a different identification to the standard occupancy category, but they all have the same importance factor (1.0), as shown in Table 4 [46]. The African codes adopt some European standards for certain specifications [47] and apply a simplified time approach (STA) and the comparable static load analysis method (ESL) to calculate the base shear of the building and distribute it among the stories. STA is given by $T = 0.05\,H^{0.75}$, where T is the structure's natural period and H is the building's height. In GB-50011, the fundamental period depends on the roof type and span, as shown in Table 4.

The nonlinearity correction coefficient (ECP-201 and RPA-99) and the ductility reduction factor (EBCS-8) modify the forces obtained from the linear analysis to reflect the nonlinear behavior. GB-50011-2010 does not apply a nonlinear response modification factor to seismic demand. Instead, it uses the equivalent factor to evaluate the possible seismic ductility of the structural element [43].

The response spectrum (for the four codes) was calculated using the soil classification and earthquake moduli values from Table 4 and are displayed in Figure 6, respectively. Schematic representations of the four-code horizontal design response spectra are also included in Table 4. The diagrams show the limit, lowest, maximum, and intermediate T values. Three intervals can be separated out of Figure 6: (1) The first varies from 0.2 to 0.7 s, and the coding sequence is ECP-201, EBCS-8, RPA-99, GB-50011, depending on the degree of conservatism. Finally, the third interval, which starts at 2 s and shows a striking disparity of the bottom bounds of the four codes where ECP-201 conservatism outperformed the other codes, ranges from 0.7 to 2 s. This comparison of design response spectra, according to El-Kholy et al. [48] may be misleading if other elements, including time T, seismic weights W, and cracking stiffness ratios, are not considered. As observed in Figure 6, the response spectrum of ECP-201 surpasses that of the other codes. As observed in Figure 6, the response spectrum of ECP-201 surpasses that of the other codes. This is attributed to ECP-201's implementation of the response spectrum method, which features pseudo acceleration linked to the PGA. Additionally, the soil parameter significantly impacts the shape of the response spectrum curve, further influencing the results. This highlights the importance of considering soil parameters in seismic analysis [10].

The probability that ground motions will cause damage depends on several variables, including the ground motion's acceleration, period, and amplitude, the structures' dynamic properties, and the ground acceleration's frequency content. Due to the characteristics of ground motion records, ground acceleration factors might differ greatly. Different sets of seismic records that correspond to the design response spectra of the structure site are used to estimate this discrepancy. As illustrated in Table 4.

where ω: behavior factor;

ω_0: the basic value of the behavior factor dependent on the structural type;

k_D: ductility factor;

$k_{R.}$: structural regularity in elevation factor;

k_w: factor reflecting the prevailing failure made in structural type;

ψ_1: the roof-type building;

l: span of the building;

C_t: coefficient, the function of the lateral force-resisting system;

H: height measured in meters from the basis of the structure to the top of the last level (N);

$\gamma = 0.9 + 0.05 - \frac{\zeta}{0.3} + \zeta$, $\eta_1 = 0.02 + 0.05 - \frac{\zeta}{4} + 32\zeta$, $\eta_2 = 1.0 + 0.05 - \frac{\zeta}{0.08} + 1.6\zeta$;

W_{Gi} weight due to the dead loads and loads of the eventually fixed equipment attached to the structure;

W_{Qi} live loads;

β weighting coefficient, depending on the nature and the duration of the live load;

λ correction factor; and

G_{EK} equivalent gravity loads.

The four standards specify that the seismic mass represents the dead load plus a fraction of the live load based on the occupation category. ECP-201, EBCS-8, and RPA-99 correlate the relationship between occupied levels and the occupancy category. ECP-201 and EBCS-8 stipulate $w = 0.25$ for office buildings with independently occupied floors. RPA-99 is multiple live loads by weight factor based on the natural duration of the live load. In GB-50011, the total dead load of the building plus 0.5 times the live load is shown in Table 4.

Table 4 contains the basic shear base resistance formulae for the Chinese and African standards. The basic shear computation can be used for shorter vertically homogenous constructions in GB-50011-2010 (i.e., where mass and stiffness are distributed uniformly in the vertical direction). The seismic impact coefficient affects the earthquake strength, site categorization, peak acceleration, and damping ratio.

4. Seismic Performance Assessment

4.1. Vibration Modes. The Ritz method [49] was used to analyze the models of the four structures. The Ritz method is a direct numerical method for finding eigenvalues linked to a structure's modal shapes and natural frequencies. The analysis included the effects of crack flexural rigidity, specific seismic mass, and shear diaphragms on the structure's dynamic behavior. Figure 7 shows the modal shapes in the X direction (short span) for different frames. Figure 7(a) shows two mode shapes for the 2-story frame. Figure 7(b)–7(d) show the first four modal shapes for the 4-, 8-, and 12-story frames, respectively. There is a very small difference between frames designed by Chinese and African codes due to mass and the cross-section of the members, which changed their stiffness and mass properties.

4.2. Base Shear. Base shear refers to the maximal lateral force exerted at the base of a building by the ground motion, as shown in Figure 8. illustrates the time history of the base shear due to the Coalinga ground motion. Specifically, Figure 8(a)–8(d) represent the base shear for 2-, 4-, 8-, and 12-story frames, respectively. These frames are designed

Table 4: Comparison of seismic provisions.

	GB-50011	ECP-201	EBCS-8	RPA-99
Soil type	D	C	C	S_3
Seismic zone and intensity	8 $a_g = 0.20\,g$	Fourth $a_g = 0.20\,g$	Fourth $a_g = 0.20\,g$	IIa $a_g = 0.20\,g$
Seismic and soil factors	$\zeta_a = 1.3$	$S = 1.5$	$S = 1.15$	
Importance factor	$I = 1$	$I = 1$	$I = 1$	$I = 1$
Response modification factor	No special factor	$R = 5$	$\omega = k_D k_R k_w$ $\gamma_0 = 0.3$ $k_D, k_R, k_w = 1$	$R = 5$
Fundamental time period, T (s)	$T = 0.23 + 0.0025\psi_1 l\sqrt{H^3}$	$T = C_t H^{3/4}$	$T = C_t H^{3/4}$	$T = C_t H^{3/4}$
Response spectrum	$(I)\ \alpha = [(10\eta_2 - 4.5).T + 4.5].\alpha_{\max}$ $(II)\ \alpha = \eta_2.\alpha_{\max}$ $(III)\ \alpha = (\frac{T_g}{T})^{\gamma}\,\eta_2.\alpha_{\max}$ $(IV)\ \alpha = [\eta_2 0.2^{\gamma} - \eta_1.(T - 5T_g)].\alpha_{\max}$	$(I)\ S_e(T) = a_g.S.[1 + \frac{T}{T_b}.(\eta.2.5 - 1)$ $(II)\ S_e(T) = a_g.S.\eta.2.5$ $(III)\ S_e(T) = a_g.S.\eta.2.5\,[\frac{T_c}{T}]$ $(IV)\ S_e(T) = a_g.S.\eta.2.5\,[\frac{T_c T_g}{T^2}]$	$(I)\ S_e(T) = a_g.S.[1 + \frac{T}{T_b}.(\eta.2.5 - 1)$ $(II)\ S_e(T) = a_g.S.\eta.2.5$ $(III)\ S_e(T) = a_g.S.\eta.2.5\,[\frac{T_c}{T}]$ $(IV)\ S_e(T) = a_g.S.\eta.2.5\,[\frac{T_c T_g}{T^2}]$	$(I)\ \frac{S_a}{g} = 1.25A\,(1 + \frac{T_1}{T}(2.5\eta\frac{Q}{R} - 1))$ $(II)\ \frac{S_a}{g} = 2.5\eta\,(1.25A\frac{Q}{R})$ $(III)\ \frac{S_a}{g} = 2.5\eta\,(1.25A\frac{Q}{R})(\frac{T_2}{T})^{2/3}$ $(IV)\ \frac{S_a}{g} = 2.5\eta\,(1.25A\frac{Q}{R})(\frac{T_2}{T})^{3/2}(\frac{T_2}{T})^{5/3}$
Story drift	$d_r \le 1/550\,h$	$d_r \le 0.005\,h$	$d_r \le 0.015\,h$	$d_r \le 0.01\,h$
Seismic weight, W	$W_{Gi} + 0.5W_{Qi}$	$W_{Gi} + 0.25\,W_{Qi}$	$W_{Gi} + 0.25W_{Qi}$	$W_{Gi} + \beta W_{Qi}$
Base shear	$F_{EK} = (\frac{T_g}{T})^{\gamma}\eta_2\alpha_{\max}G_{EK}$	$F_b = S_e(T)\lambda W/g$	$F_b = S_e(T)W$	$F_b = S_e(T)\lambda W$

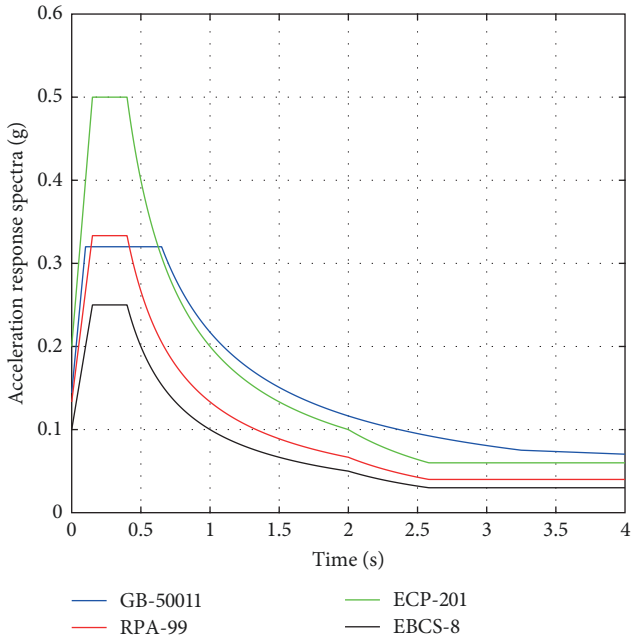

Figure 6: Horizontal spectrum curves for the site and building guide in the four codes examined.

according to four different seismic codes: EBCS-8, ECP 201, RPA 99, and GB-50011.The results for African code are almost same. Figure 8(d) shows that for the 12-story frame, the peak base shear values obtained from ECP-201, EBCS-8, and RPA-99 codes are 6,073 kN, and the peak base shear for GB-50011 is 7,445 kN. A similar trend is observed for other frames, where the GB-50011 code gives the highest base shear estimation compared to other regulations. This indicates that the GB-50011 code is more conservative and may result in the overdesign of structures due to the design of the response spectrum, as shown in Figure 6, and the seismic weight.

4.3. Story Shear Force. This section examined how frame rigidity affects the shear distribution in buildings of different heights. The frames were analyzed using time history for nine earthquake records. The time history method integrates the equations of motion for a multidegree of freedom using nine ground motion acceleration records. Figure 9 shows the results of the analysis. It reveals that the story shear demands depend on the lateral stiffness of the frames, which increases with higher stiffness. Figures 9(c) and 9(d) also indicate that the story shear values for GB-50011 are overestimated. The African code has the same results suggesting that these codes have comparable assumptions and criteria for the frame design.

4.4. Interstory Drift. Interstory drift ratio (IDR) reflects the degree of structural damage that can occur during an earthquake. The data obtained from the time-history response was used to determine the greatest relative displacements between each floor (for every story level). Following this, the interstory drifts ratio were computed by taking the ratio of these maximum relative displacements to their corresponding story heights. Figure 10 shows the IDR values for the model frames under different seismic codes. The lateral load pattern causes a significant soft-story effect, particularly for the building based on the GB-50011 standard. This effect is more pronounced for the 2-, 4-, 8-, and 12-story frames, which have a maximum IDR of 0.44%, which is still within the allowable limit. It can also be observed that the largest IDR values are located in the middle stories of the frames. On the contrary, the other codes, namely ECP-201, RPA-99, and EBCS-8, tend to underestimate the IDR values compared to the GB-50011 code.

4.5. Pushover Analysis. The criteria pushover analysis used to compare the performances are the strength ratio, R, and the ductility, μ, of the frames. The strength ratio is defined as the ratio of the base shear force to the structure's weight, and the ductility refers to the ratio of the maximum displacement to the elastic displacement of the structure. These metrics are calculated from the nonlinear static analysis of the frames under different seismic intensity levels. Figure 11 visually compares the strength ratio and ductility curves for two of the 4-story frame structures considered in this study designed by the African and Chinese codes. The method a tends to overestimate the structure's strength and ductility for a given seismic intensity, resulting in a conservative design. In Figure 11, 16%, 50%, and 84% are typically indicative of statistical metrics employed in probabilistic seismic demand models. The 16% fractile signifies a lower limit, the 50% fractile corresponds to the median, and the 84% fractile denotes an upper limit. These fractiles serve as critical markers in understanding the distribution and potential variability of seismic demands. Especially, Figure 11 indicates that frame design by African code has more probability of seismic demand compared to the frame design by the GB-50011 is more effective and reliable for designing RC frames under seismic loading.

4.6. Fragility Curves. Fragility curves are graphical tools used to evaluate the potentiality of structural damage under various levels of earthquake intensity. In seismic fragility analysis, the mean and standard deviation values are derived from a statistical examination of the outcomes from the time-history IDA. This process involves calculating the roof drift associated with various damage states—namely; OP, IO, DC, LS, and CP. These states correspond to specific values: 0.5%, 1%, 1.5%, 2%, and 2.5%, respectively. The fragility curves are shown in Figure 12 for four performance levels (OP, IO, DC, LS, and CP). The results indicate that all the model frames have a full probability (100%) to reach or exceed the OP-level under certain ground motion intensities. These intensities are 0.8, 0.77, 0.7, and 0.3 g for the frames designed by EBCS-8, ECP-201, RPA-99, and GB-50011 codes, respectively. The frame designed by the GB-50011 code will experience at least IO-level damage when a 0.75 g ground motion is applied. Similarly, the results show that the probability reach or exceed the LS-level varies among the frames under a 1.5 g ground motion. The frame designed by the GB-50011 code has a full probability (100%) to reach or exceed the DC-level, while the frames designed by EBCS-8, RPA-99, and GB-50011 codes have lower possibilities of 38%, 34%, and

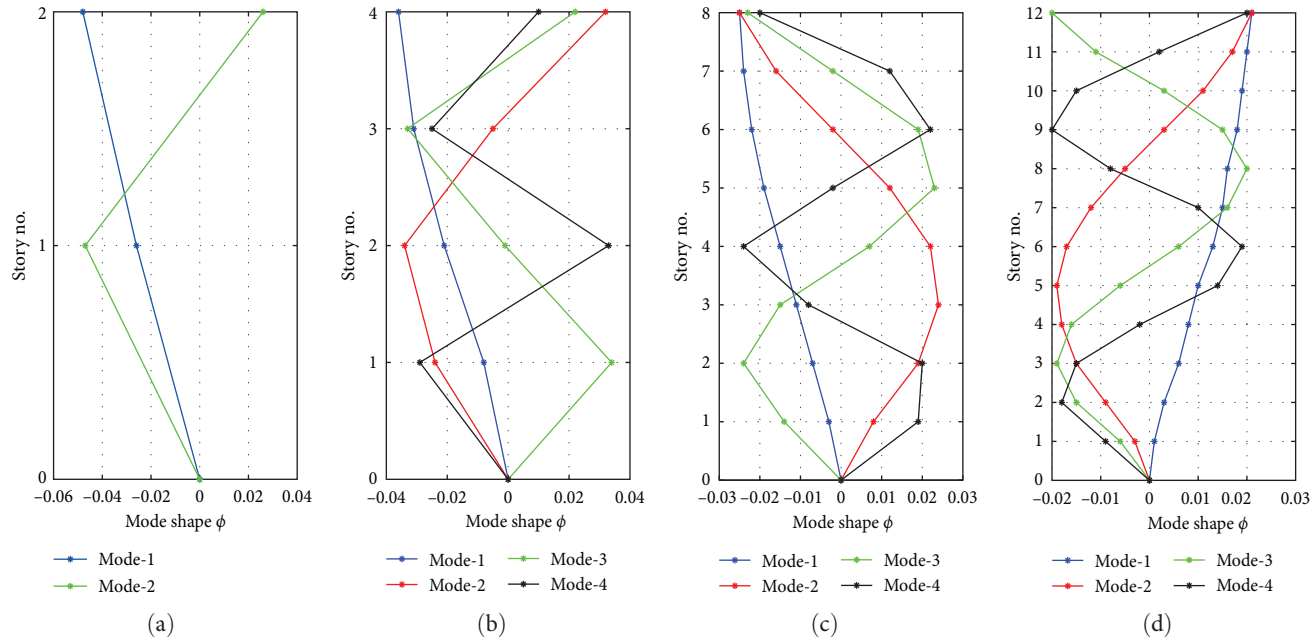

Figure 7: Mode shapes (X direction): (a) 2-story; (b) 4-story; (c) 8-story; and (d) 12-story.

35%, respectively. Figure 12 observe that the buildings designed according to GB-50011 exhibited different standard deviations in the fragility curves. This is attributed to the greater roof drifts observed for these buildings. The IDA outcomes indicated that the response of the GB-50011 designed buildings, in terms of both interstory drifts and story shear, was greater when compared to those designed by African codes. This finding is consistent with the observed ductility capabilities of the structures, as illustrated in Figure 11, where GB-50011 designed buildings show a smaller ductility capability.

4.7. Total Energy Components. Total energy components show how energy is divided among different structure parts during seismic analysis. The energy components are input energy, kinetic energy, potential energy, and damping energy, Table 5 shows the maximum value of the energy components. Input energy is the energy given to the structure by an external seismic load [50]. Kinetic energy is the energy related to the movement of the structure, this indicates the possibility of structural damage [51]. Potential energy is the energy saved in the structure due to the elastic stress that can be released when the load is removed. The damping energy is the energy the structure loses because of damping mechanisms, such as material damping or Rayleigh damping [51].

5. Discussion

(1) Different codes and standards have different methods and criteria for estimating the base shear. The paper shows that among the four codes considered, GB-50011 gives the highest base shear estimation for all frames, regardless of their height or number of stories. This means that the GB-50011 code is more conservative and may result in the overdesign of structures. On the other hand, the peak base shear values obtained from ECP-201, ECBS-8, and RPA-99 are relatively close, indicating that these codes have similar assumptions and factors for estimating the base shear.

(2) The story shear demands four frames of different heights using time-history analysis methods. The paragraph shows that the story shear demands increase with the frame stiffness and that the ECP-201, RPA-99, and EBCS-8 codes give similar results, while the GB-50011 code gives higher results.

(3) The buildings' IDR values using different seismic codes. The paragraph shows that GB-50011 gives the highest IDR values, as expected due to the design response spectrum seismic weight estimation, which indicates a soft-story effect, while the ECP-201, RPA-99, and EBCS-8 codes tend to underestimate the IDR values compared to the GB-50011 code.

(4) This study developed fragility curves for four model frames based on four seismic codes. The results of the fragility analysis indicate that the GB-50011 code is the most conservative, as it gives the highest probability of damage for all performance levels. This means that the frame designed by this code is more likely to experience structural damage than the other frames under the same ground acceleration intensity. On the other hand, the African codes are the least conservative, as they give the lowest probability of damage for all performance levels. This means the frame designed by these codes is more resilient and can withstand higher ground motion intensities without significant structural damage.

(5) Based on this study, we discovered that the seismic design codes of Africa are derived from the European

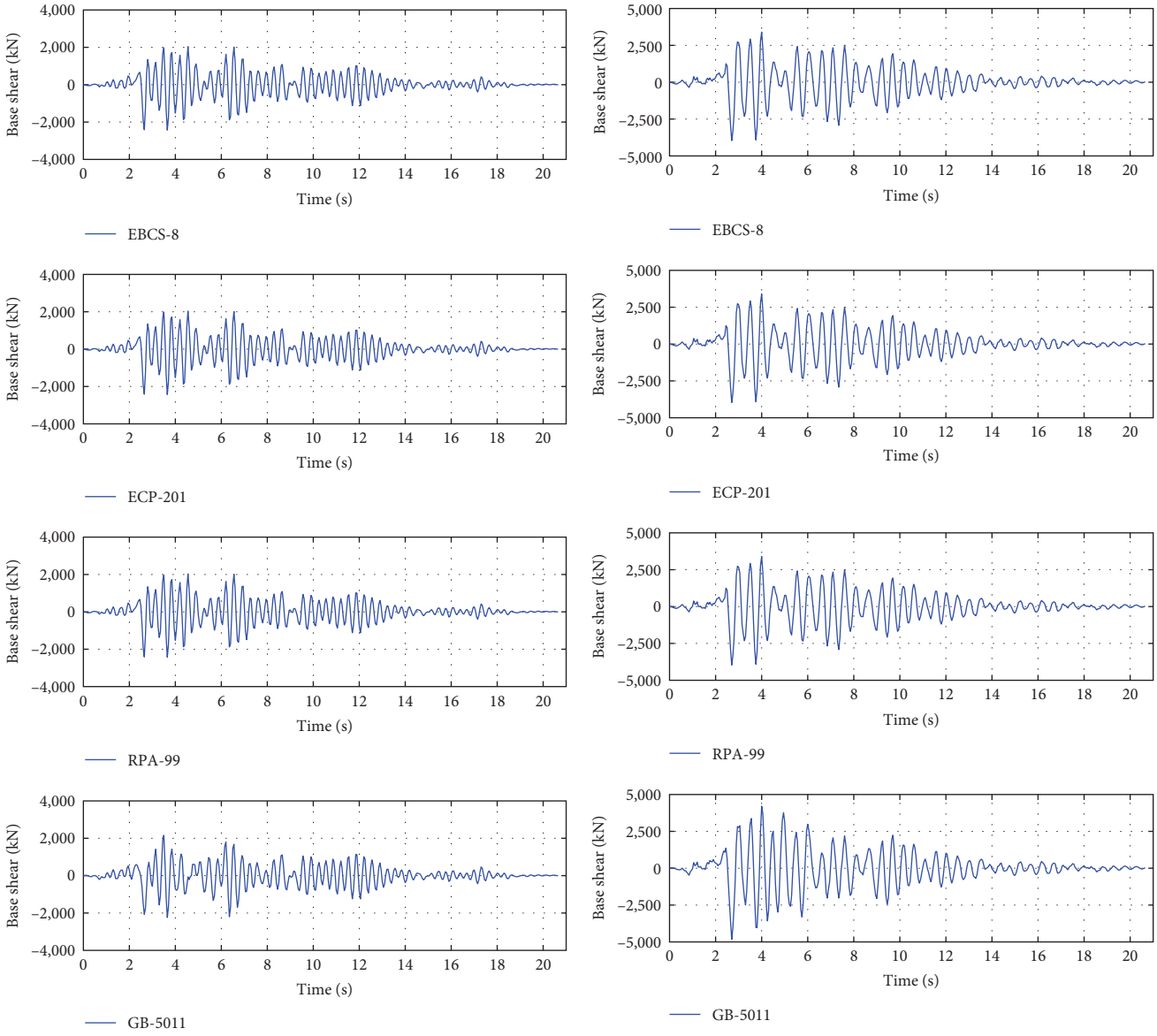

Figure 8: Continued.

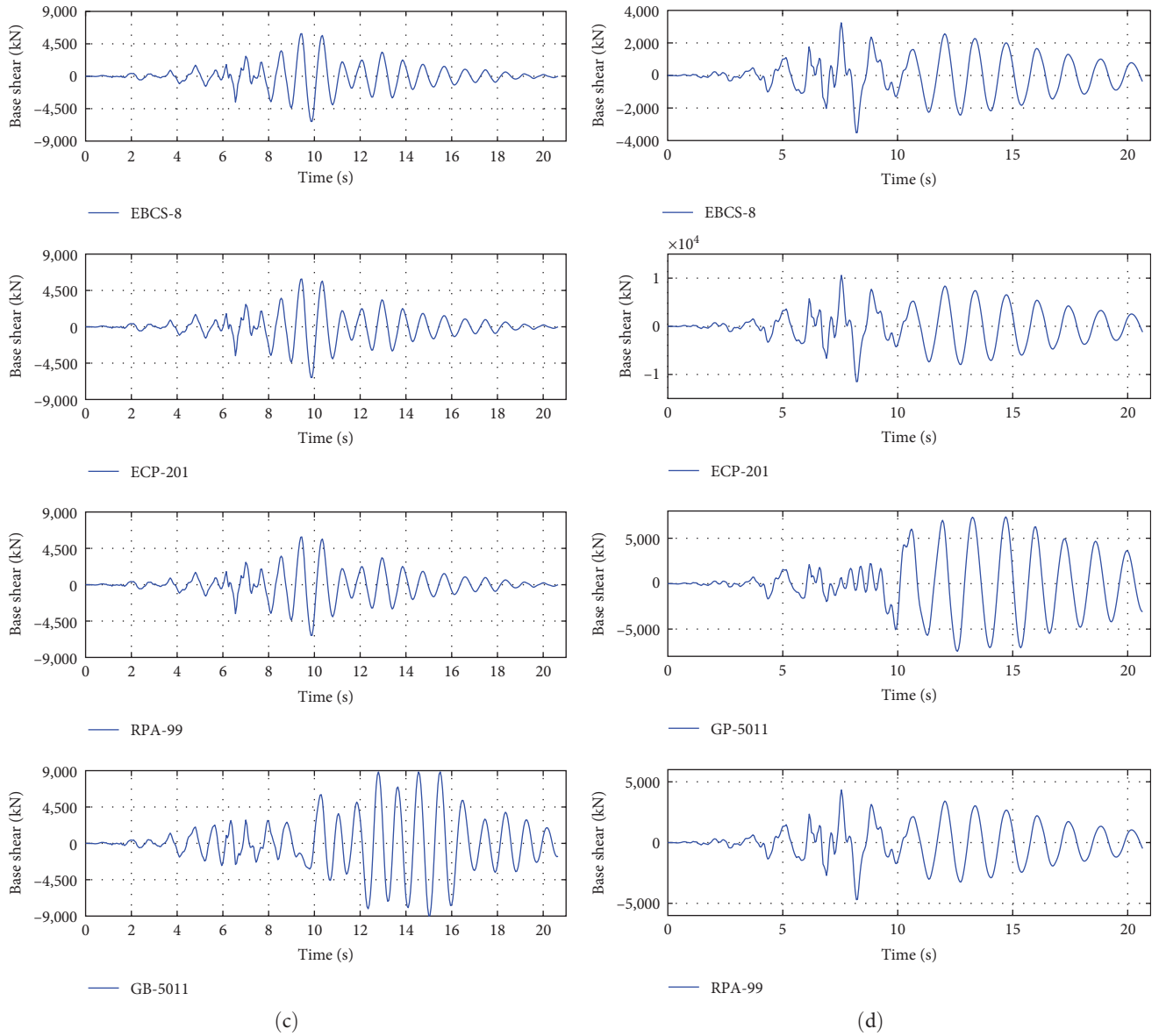

Figure 8: Base shear due to Coalinga ground motion: (a) 2-story; (b) 4-story; (c) 8-story; and (d) 12-story.

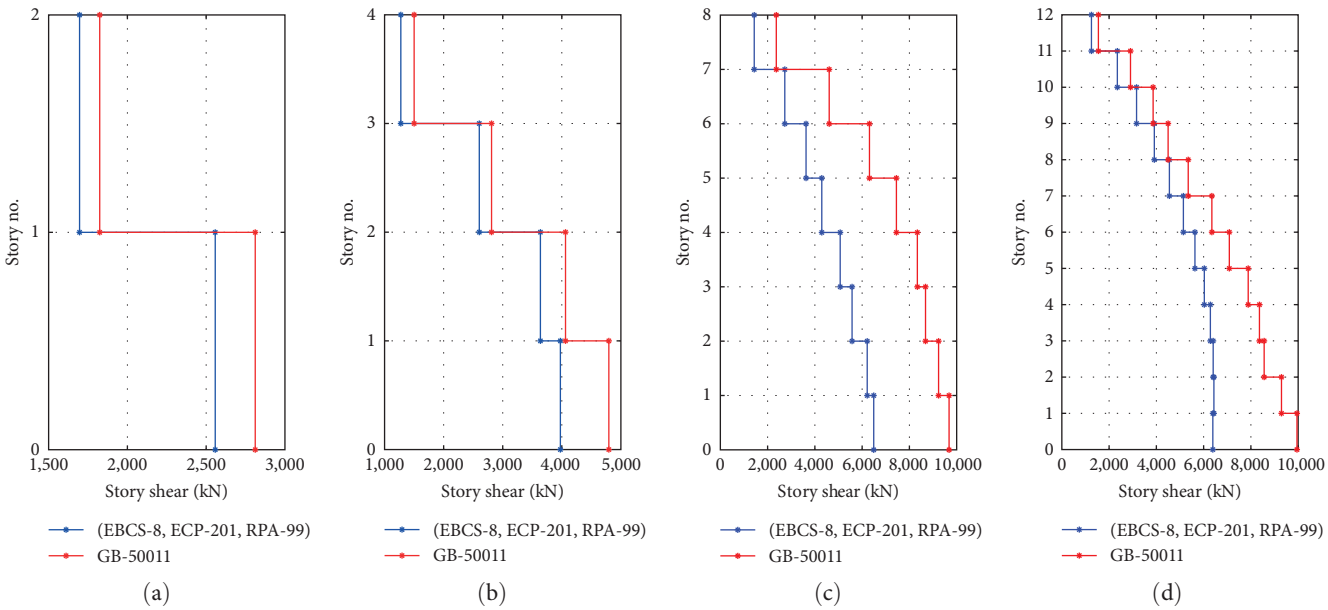

Figure 9: Story shear force: (a) 2-story; (b) 4-story; (c) 8-story; and (d) 12-story.

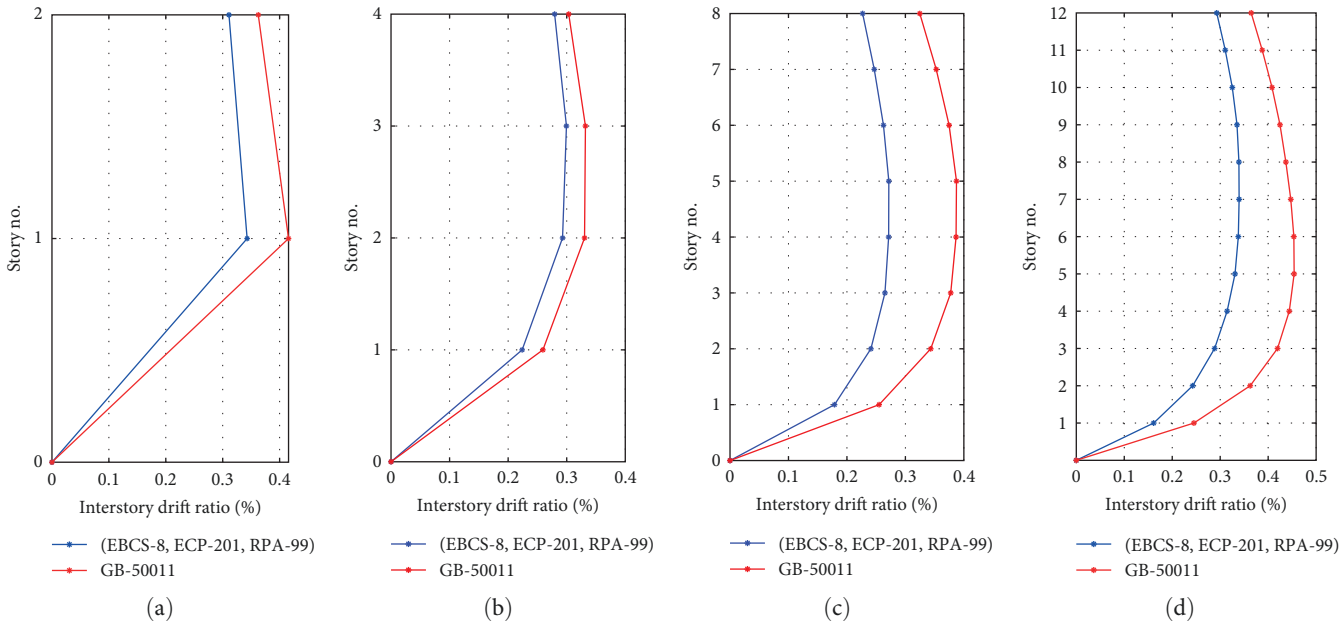

Figure 10: Interstory drift ratio (%): (a) 2-story; (b) 4-story; (c) 8-story; and (d) 12-story.

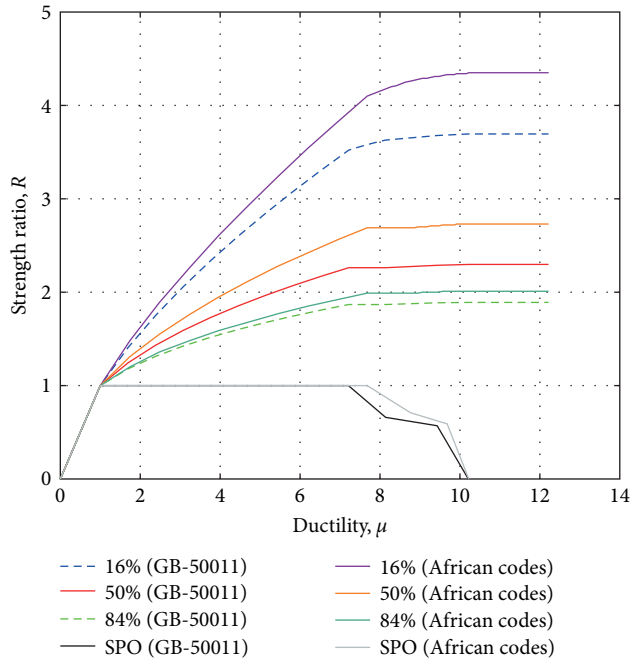

Figure 11: Comparison of the strength ratio to ductility response due to pushover analysis of 4-story frame.

code 8, and most of the provisions of the African code follow the same procedures. The main differences between these codes lie in the soil classifications and the design response spectrum. We obtained similar results for these codes when we performed the same ground motion scaling for time-history analysis.

(6) This research reveals that China's seismic design code exceeds the African code by 20%. Since the Chinese companies have engineering projects in Africa, they can apply the Chinese code by considering the soil classifications in Africa. This excess results from the fact that the estimation of seismic weight needs to be adjusted to meet the African design criteria.

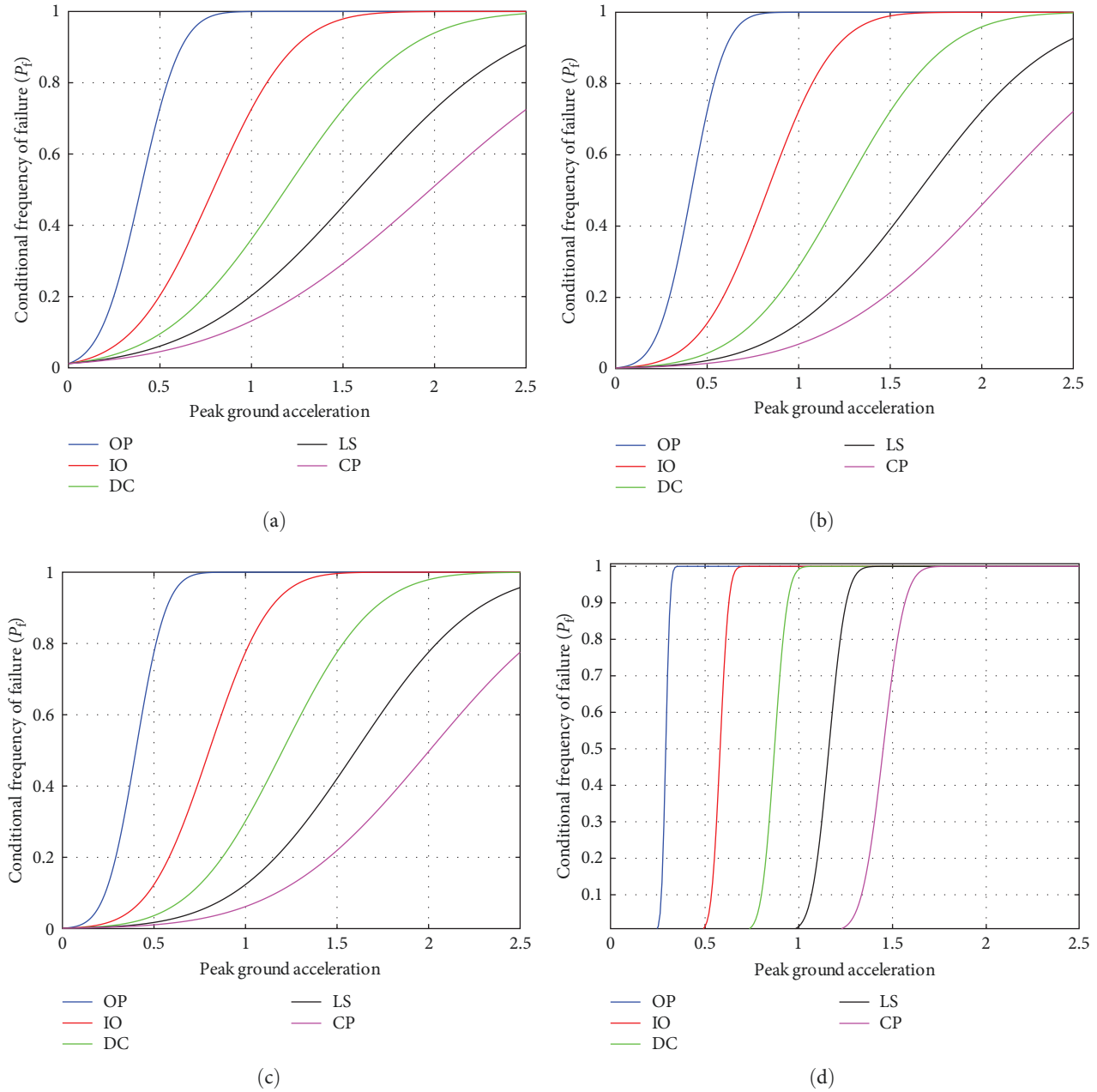

FIGURE 12: Fragility curve of 12-story frame: (a) EBCS-8; (b) ECP-201; (c) RPA-99; and (d) GB-50011.

6. Conclusions

This paper compares the earthquake performance evaluation of MRF-RC frame buildings using four different codes: Ethiopian Building Code Standard (EBCS-8), Egyptian Code for Design and Construction of Reinforced Concrete Structures (ECP-201), Algerian Seismic Monitoring Code Regulations (RPA 99), and the Chinese Code for Seismic Design of Buildings (GB-50011). The study designs 2-, 4-, 8-, and 12-story RC model frames according to the four-code amplitude design principle. It then compares and presents the four-code seismic criteria for soil classification, seismic zone, response modification, response spectrum, story drift, seismic weight, and base shear. The study also evaluates the earthquake behavior of the model frames by IDA and NL-THA using different ground acceleration levels and provisions given in EBCS-8, ECP-201, RPA-99, and GB-50011. Moreover, the study identifies and summarizes some major differences among the four codes:

(1) The African code for seismic design: EBCS-8, ECP-201, and RPA-99, these standards are based on the European seismic code (Eurocode-8), which provides general principles and rules for designing structures to resist earthquakes. Most of the equations and provisions in the African codes are the same as those in

Table 5: Total energy components.

Frame	Codes	Input energy (kN·m)	Kinetic energy (kN·m)	Potential energy (kN·m)	Global damping energy (kN·m)
12-Story	EBCE-8	1,914.5129	387.8569	312.3853	1,886.0458
	ECP-201	1,914.6198	387.868	312.4183	1,886.1516
	RPA-99	1,914.6771	387.8782	312.4305	1,886.2049
	GB-50011	3,440.5211	730.7788	668.8212	2,950.4465
8-Story	EBCE-8	1,208.5109	220.8478	171.9942	1,189.8422
	ECP-201	1,208.4573	220.837	171.9905	1,189.7964
	RPA-99	1,208.4573	220.837	171.9905	1,189.7964
	GB-50011	1,392.9208	366.0605	391.5282	1,385.9667
4-Story	EBCE-8	559.8891	105.0225	100.3221	553.2
	ECP-201	559.8597	105.0151	100.3147	553.1709
	RPA-99	559.89	105.02	100.3184	553.2004
	GB-50011	589.1035	133.7471	127.5232	589.0172
2-Story	EBCE-8	212.1511	43.2582	41.7823	211.9467
	ECP-201	212.1607	43.2588	41.7841	211.9563
	RPA-99	212.1616	43.2578	41.7835	211.9572
	GB-50011	225.9305	55.3473	52.8576	224.0491

Eurocode-8, with only minor modifications. The main differences between the three codes lie in the soil classification and seismic zonation. The African codes adopt a different system of classifying soil types according to their geotechnical properties and seismic response. The African codes also divide the continent into different seismic zones depending on the expected earthquake hazard level and ground acceleration. This would facilitate the unification process of seismic design codes for African countries.

(2) Based on preliminary research, developing a unified African seismic design code is essential. Since the existing African codes are derived from the European code, this would facilitate the unification process by considering the soil classification and seismic zones for the whole of Africa. This would bring significant benefits to African countries and reduce costs compared to creating standards for individual countries. Moreover, some African countries lack codes for seismic design.

(3) This study has compared the seismic performance of moment resisting frames designed based on Chinese and African codes using different metrics, such as base shear, story shear, IDR, and fragility curves. The results show significant differences between these codes regarding the safety and resilience of structures under seismic actions. This is an important finding for Chinese engineering firms increasingly involved in international projects under the "One Belt and Road Initiatives" proposal, as they need to understand and comply with international design standards. Based on this research, the Chinese engineering frame can use the Chinese seismic design code in their projects in Africa for some parameters like soil classifications in Africa. However, this study has some limitations, as it only considers one type of structure. Therefore, future research could extend such comparison to different structures, such as steel frames, shear walls, or braced frames, to further investigate the strengths and weaknesses of Chinese and African codes for seismic design.

Data Availability

The data that have been used to support the results of this study are contained in the article.

Conflicts of Interest

The authors declare that they have no conflicts of interest.

Acknowledgments

The authors greatly appreciate the support from the Chinese Scholarship Council (CSC).

References

[1] D. Zhiquan, W. Zhizhao, L. Bo, H. Zhang, and H. A. Aziz, "General comparison of seismic design between the Chinese code and the European code," *E3S Web of Conferences*, vol. 276, Article ID 01031, 2021.

[2] The National Standard GB50011, "Code for seismic design of buildings, ministry of housing and urban-rural development of China," Beijing, China, 2010.

[3] H. U. Yuxian, "Development of earthquake engineering in China," in *13th World Conference on Earthquake Engineering*, Vancouver, B.C., Canada, 2004.

[4] M. Brandt, "Seismic hazard in South Africa council for geoscience report number: 2011-0061," 2011, (accessed April 14, 2023), https://www.geoscience.org.za/images/geohazard/seismicity.pdf.

[5] M. Meghraoui, A. Harbi, and H. M. Hussein, "Preface to the special issue "seismotectonics and seismic hazards in North Africa," *Journal of Seismology*, vol. 18, pp. 203-204, 2014.
[6] A. E. Khalil, A. Deif, and H. E. A. Hafiez, "Seismic hazard assessments at Islamic Cairo, Egypt," *Journal of African Earth Sciences*, vol. 112, pp. 287–298, 2015.
[7] H. S. Badawi and S. A. Mourad, "Observations from the 12 October 1992 Dahshour earthquake in Egypt," *Natural Hazards*, vol. 10, no. 3, pp. 261–274, 1994.
[8] M. Wilks, A. Ayele, J.-M. Kendall, and J. Wookey, "The 24th january 2016 Hawassa earthquake: implications for seismic hazard in the main Ethiopian rift," *Journal of African Earth Sciences*, vol. 125, pp. 118–125, 2017.
[9] K. K. Alaneme and E. A. Okotete, "Critical evaluation of seismic activities in Africa and curtailment policies–a review," *Geoenvironmental Disasters*, vol. 5, no. 1, Article ID 24, 2018.
[10] S. E. A. Raheem, "Evaluation of Egyptian code provisions for seismic design of moment-resisting-frame multi-story buildings," *International Journal of Advanced Structural Engineering*, vol. 5, no. 1, Article ID 20, 2013.
[11] ECL Committee, "Egyptian code for calculating loads and forces in structural work and masonry," Cairo, Egypt, 2012.
[12] K. A. Abdel-Raheem, S. E. Abdel Raheem, H. M. Soghair, and M. H. Ahmed, "Evaluation of seismic performance of multistory buildings designed according to Egyptian code," *JES. Journal of Engineering Sciences*, vol. 38, no. 2, pp. 381–402, 2010.
[13] National Center of Applied Research in Earthquake Engineering, "Algerian earthquake resistant regulations," Algiers, Algeria, 2003.
[14] S. Zermout, F. Bakhti, Y. Mehani, M. Inukai, T. Azuhata, and T. Saito, "Seismic vulnerability of a strategic building designed by algerian seismic CODE RPA 99 using the capacity spectrum method," in *The 14th World Conference on Earthquake Engineering*, pp. 1–8, WCEE, Beijing, China, 2008.
[15] Ethiopia Ministry of Construction, "EBCS-8 design of structures for earthquake resistance," Addis Ababa, Ethiopia, 1995.
[16] A. Worku, "The status of basic design ground motion provisions in seismic design codes of sub-Saharan African countries: a critical review," *Journal of the South African Institution of Civil Engineering*, vol. 56, no. 1, pp. 40–52, 2014.
[17] E. Kueht and M. B. Hueste, "Impact of code requirements in the central united states: seismic performance assessment of a reinforced concrete building," *Journal of Structural Engineering*, vol. 135, pp. 404–413, 2009.
[18] T. B. Panagiotakos and M. N. Fardis, "Seismic performance of RC frames designed to eurocode 8 or to the greek codes 2000," *Bulletin of Earthquake Engineering*, vol. 2, no. 2, pp. 221–259, 2004.
[19] N. Ile and J. M. Reynouard, "Non linear analysis of reinforced concrete shear wall under earthquake loading," *Journal of Earthquake Engineering*, vol. 4, no. 2, pp. 183–213, 2000.
[20] Y. Sheisheng, H. Xiaoqian, and Q. Rong, "Evaluation and study for earthquake resistant capability of reinforced concrete frame structure," *Earthquake Engineering and Engineering Vibration*, vol. 25, 2005.
[21] L. Ye, X. Lu, Q. Ma, X. Wang, and Z. Miao, "Nonlinear analytical models, methods and examples for concrete structures subject to earthquake loading," *Engineering Mechanics (in Chinese)*, 2006.
[22] L. Young, W. Xueping, W. Feng, and B. Shaoliang, "Comparison between seismic performances of RC frames designed according to Chinese and European Codes," *Earthquake Engineering and Engineering Vibration*, 2007.
[23] N. Gerrard, "Why have Chinese construction firms become so influential in Africa? International construction," 2023, (accessed November 30, 2023), https://www.international-construction.com/news/why-have-chinese-construction-firms-become-so-influential-in-africa-/8026251.article.
[24] Xinhua, "Chinese company to build tallest building in East Africa, China daily," 2015, (accessed November 30, 2023), https://www.chinadaily.com.cn/business/2015-04/29/content_20580309.htm.
[25] K. Getachew, D.-H. Chen, and G. Peng, "Seismic performance evaluation of RC Frame Designed using Ethiopian and Chinese seismic codes," *Advances in Civil Engineering*, vol. 2020, Article ID 8493495, 24 pages, 2020.
[26] Department of Homeland Security Emergency Preparedness and Response Directorate FEMA, "Multi-hazard loss estimation methodology earthquake model HAZUS®MH MR4 technical manual," Federal Emergency Management Agency, Washington, D.C., USA, 2003.
[27] Inc. Computers & Structures, "CSI analysis reference manual for SAP2000," 2016, (accessed April 19, 2023), https://wiki.csiamerica.com/display/doc/CSI+Analysis+Reference+Manual.
[28] M. A.-B. Abdo, "Modeling of shear-wall dominant symmetrical flat-plate reinforced concrete buildings," *International Journal of Advanced Structural Engineering*, vol. 4, no. 1, Article ID 2, 2012.
[29] D. Vamvatsikos and C. A. Cornell, "Incremental dynamic analysis," *Earthquake Engineering & Structural Dynamics*, vol. 31, no. 3, pp. 491–514, 2002.
[30] M. M. Kassem, F. M. Nazri, and E. N. Farsangi, "The seismic vulnerability assessment methodologies: A state-of-the-art review," *Ain Shams Engineering Journal*, vol. 11, no. 4, pp. 849–864, 2020.
[31] F. M. Nazri and N. A. Alexander, "Predicting the collapse potential of structures," in *Proceedings of the 15th World Conference on Earthquake Engineering*, pp. 1–9, WCEE, Lisbon, Portugal, 2012.
[32] J. Hancock, J. Watson-Lamprey, N. A. Abrahmsan et al., "An improved method of matching response spectra of recorded earthquake ground motion using wavelets," *Journal of Earthquake Engineering*, vol. 10, no. sup001, pp. 67–89, 2006.
[33] L. Al Atik and N. Abrahamson, "An improved method for nonstationary spectral matching," *Earthquake Spectra*, vol. 26, no. 3, pp. 601–617, 2010.
[34] V. Manfredi, A. Masi, A. G. Özcebe, R. Paolucci, and C. Smerzini, "Selection and spectral matching of recorded ground motions for seismic fragility analyses," *Bulletin of Earthquake Engineering*, vol. 20, no. 10, pp. 4961–4987, 2022.
[35] A. Kaveh and V. R. Mahdavi, "A new method for modification of ground motions using wavelet transform and enhanced colliding bodies optimization," *Applied Soft Computing*, vol. 47, pp. 357–369, 2016.
[36] T. Takeda, M. A. Sozen, and N. N. Nielsen, "Reinforced concrete response to simulated earthquakes," *Journal of the Structural Division*, vol. 96, no. 12, pp. 2557–2573, 1970.
[37] H. M. Dwairi, M. J. Kowalsky, and J. M. Nau, "Equivalent damping in support of direct displacement-based design," *Journal of Earthquake Engineering*, vol. 11, no. 4, pp. 512–530, 2007.
[38] A. Louzai and A. Abed, "Evaluation of the seismic behavior factor of reinforced concrete frame structures based on comparative analysis between non-linear static pushover and

incremental dynamic analyses," *Bulletin of Earthquake Engineering*, vol. 13, no. 6, pp. 1773–1793, 2015.

[39] D. Vamvatsikos and C. A. Cornell, "Direct estimation of seismic demand and capacity of multidegree-of-freedom systems through incremental dynamic analysis of single degree of freedom approximation," *Journal of Structural Engineering*, vol. 131, no. 4, pp. 589–599, 2005.

[40] P. Fema, "Commentary for the seismic rehabilitation of building," FEMA-356, Federal Emergency Management Agency, Washington, DC, 2000.

[41] H. B. Kaushik, D. C. Rai, and S. K. Jain, "Effectiveness of some strengthening options for masonry-infilled RC frames with open first story," *Journal of Structural Engineering*, vol. 135, no. 8, pp. 925–937, 2009.

[42] A. T. Council, "Seismic evaluation and retrofit of concrete buildings," Report No, SSC 96-01: ATC-40 1, 1996.

[43] H. Duan and M. B. D. Hueste, "Seismic performance of a reinforced concrete frame building in China," *Engineering Structures*, vol. 41, pp. 77–89, 2012.

[44] Applied Technology Council, "Quantification of building seismic performance factors: component equivalency methodology, federal emergency management agency," Washington, D.C., USA, 2011.

[45] Y. E. Ibrahim and M. M. El-Shami, "Seismic fragility curves for mid-rise reinforced concrete frames in Kingdom of Saudi Arabia," *The IES Journal Part A: Civil & Structural Engineering*, vol. 4, no. 4, pp. 213–223, 2011.

[46] S. S. F. Mehanny and H. A. El Howary, "Assessment of RC moment frame buildings in moderate seismic zones: evaluation of Egyptian seismic code implications and system configuration effects," *Engineering Structures*, vol. 32, no. 8, pp. 2394–2406, 2010.

[47] The European Standard EN, "Eurocode 8: design of structures for earthquake resistance," 2004.

[48] A. M. El-Kholy, H. Sayed, and A. A. Shaheen, "Comparison of Egyptian code 2012 with Eurocode 8-2013, IBC 2015 and UBC 1997 for seismic analysis of residential shear-walls RC buildings in Egypt," *Ain Shams Engineering Journal*, vol. 9, no. 4, pp. 3425–3436, 2018.

[49] W. Szemplinska-Stupnicka, ""Non-linear normal modes" and the generalized Ritz method in the problems of vibrations of non-linear elastic continuous systems," *International Journal of Non-Linear Mechanics*, vol. 18, no. 2, pp. 149–165, 1983.

[50] Y. H. Chai and P. Fajfar, "A procedure for estimating input energy spectra for seismic design," *Journal of Earthquake Engineering*, vol. 4, no. 4, pp. 539–561, 2000.

[51] C.-M. Uang and V. V. Bertero, "Evaluation of seismic energy in structures," *Earthquake Engineering & Structural Dynamics*, vol. 19, no. 1, pp. 77–90, 1990.